J Solid State Electrochem (2000) 4: 95–106

ORIGINAL PAPER

Tadeusz Błaszczyk · Danuta Kaźmierczak
Pawel Krzyczmonik · Henryk Scholl
Krzysztof Polański

The surface characteristics of polycrystalline cobalt electrooxidised in sulfuric acid solutions

Received: 6 January 1999 / Accepted: 5 May 1999

Abstract The oxidation of cobalt electrodes has been carried out by means of cyclic voltammetry and coulometry under controlled potential in sulfuric acid solutions of different concentrations. The electrochemical scanning tunneling microscope/scanning tunneling microscope (ECSTM/STM) systems constructed by the authors and scanning electron microscopy (SEM) with the SEM-EDX system of surface analysis of the elements have been used. The procedure applied in this work made it possible to observe the fragments of the same surface by means of SEM and ECSTM/STM. The most typical images for a polycrystalline Co electrode with a ±10% accuracy at the scales of 4800 nm × 4800 nm and 100 nm × 100 nm are presented and the results are discussed. In a diluted electrolyte (0.1 M), irregular forms of a stable cobalt oxide with Co:O ratio ~1:1 appear. Unreproducible results have been obtained in a 1.0 M H_2SO_4 solution. Compact and relatively regular layers of cobalt oxide of the same ratio have been obtained in 0.1 M H_2SO_4, as well as in 10.0 M sulfuric acid solution, under controlled oxidation potential at the passivation range.

Key words Cobalt oxides · Electrochemical scanning tunneling microscopy · Surface topography · Polycrystalline cobalt · Electrooxidation

T. Błaszczyk · D. Kaźmierczak
P. Krzyczmonik · H. Scholl (✉)
Department of General and Inorganic Chemistry,
University of Łódź,
ul. Narutowicza 68, 90-136 Łódź, Poland
e-mail: hscholl@chemul.uni.lodz.pl

K. Polański
Department of Solid State Physics,
University of Łódź,
ul. Pomorska 159/163, 90-236 Łódź, Poland

Introduction

The electronics and computer industries, aiming at miniaturisation of artificial systems, such as solid state devices and diagnostic kits, has pushed forward the development of new micro- and nano-structure manufacturing techniques [1–11]. At present, the oxide-type electrodes represent an active field of physical and electrochemical investigations. Their applications in nanotechnology or ceramic oxide materials in electrochemical technology and in nanotribology are under consideration. Simple oxides, particularly NiO, CoO and Co_2O_3, their electrochromic properties and oxidation-hydration reaction products, as well as some stable spinel-type complex oxides, have been investigated in alkaline conditions [12, 13].

The main electrophysical parameters of oxide semiconductors can be investigated experimentally by means of the band models or electrical conductivity models, by means of electron work functions (Φ_{Co} = 4.70 eV after Trasatti's selection [13]), by the quantity and mobility of current carriers, or illustrated by the forbidden band width. These parameters are highly sensitive to the chemical and structural composition of the oxide systems, and as such they essentially depend on the method and on the conditions of oxide synthesis [13, 14]. The electrical conductivity of semiconductors increases with the increase of the stoichiometry of oxygen.

Spinels, which were investigated extensively as electrodes for electrocatalytic processes [15] and – to a lesser extent – as electrochromic materials, are usually prepared by: (1) thermal procedures of surface oxides, (2) evaporation of the solutions of nitrates, (3) co-precipitation of hydroxides and oxalates, (4) cryochemical synthesis, and/or (5) an electrochemical oxidation of the metal surface in different electrolyte solutions. This type of electrode is interesting for practical applications as it is based on a cheap and easily available material which, from an electrocatalytic standpoint, offers a relatively high activity and a rather good selectivity. The oxide

Co_3O_4 is known as one of the most active catalysts that bind oxygen with a maximum reaction rate [15, 16]. The active sites in Co_3O_4 are related to a higher valence of cobalt ions balancing the cationic vacancies [17]. The formula of this oxide can be described as follows: $\{[Co(II)Co(III)]_{3-x}\blacksquare n_xO_4\}$, where ■ is the vacant lattice site.

Trasatti [13] described the properties of the Co_3O_4 spinel as follows: electrical conductivity $\kappa = 2 \times 10^{-4}$ ohm^{-1} cm^{-1}, Fermi level = 0.062 eV, hole concentration = 9.5×10^{20} cm^{-3}. The trivalent cations play an important role in heterogeneous catalysis.

Arvia and co-workers [18] obtained a porous and amorphous Co_3O_4 layer on a metallic cobalt electrode in alkaline aqueous solutions by means of combined cyclic voltammetry. The H^+/H_2 electrodes in the same solutions were used as reference systems. Differential thermal analysis showed that at least six water molecules per Co_3O_4 are involved in the overlayer structure. The electrochromic properties of Co_3O_4 films deposited on transparent glass/tin oxide electrodes and polarised in 0.1 M KOH solution were described by Maruyama and Arai [19]. They obtained a spinel structure, i.e. a structure with a mixed oxide, $Co(II)Co(III)_2O_4$, showing that the cathodic reduction $Co(III) \Rightarrow Co(II)$ is possible.

Among many electrochemical investigations of anodic dissolution, the phenomena of passivation and transpassivation at a "macroscopic" scale were investigated in the recent work of Itaya and co-workers [20]. This work was devoted to the anodic dissolution of Co(0001) single crystals at the atomic scale. Cyclic voltammetry in diluted Na_2SO_4 (pH 3) showed that the anodic dissolution of Co(0001), without passivation processes, occurs with the exposition of atomically flat terraces completely covered with clear hexagonal lattices. The Co atoms, oxidised to Co^{2+} ions, are located on the hollow sites in the layer of O^{2-} ions. It is possible that the oxide is the first adlayer of $Co(OH)_2(0001)$, with the same symmetry as that of a hexagonal oxide lattice with a lattice constant of 0.31 ± 0.01 nm.

The aim of this work is to present the formation of a polycrystalline cobalt oxide layer in aqueous sulfuric acid solutions of different concentrations and to investigate the scanning electron microscopy (SEM) surface analysis of the elements. The characteristics of the topography of the cobalt oxide layer at the nanoscale, its roughness and growth are described by means of the electrochemical scanning tunneling microscopy/scanning tunneling microscopy (ECSTM/STM) methods as well as by surface analysis of the elements using the SEM energy dispersive X-ray (SEM-EDX) method.

Experimental

The polycrystalline cobalt samples used as working electrodes were prepared from cobalt rod (Koch-Light 99.998%) with a geometric area $A_{geom} = 0.20 \pm 0.02$ cm^2. They had the form of discs, 2 mm thick, $\phi = 5$ mm. Samples were first mechanically polished using 2000 silicon carbide paper, chemically polished in a solution of 65% glacial acetic acid and 15% orthophosphoric acid [21] in the Millipore-Q RG water, and rinsed by Millipore-Q RG water deoxidised by an argon stream.

As a starting point for the electrochemical investigations of the cobalt samples at the nanoscale, the initial $\log I = f(E)$ anodic curve measurements were recorded at the scan rate $v = 0.01$ V s^{-1} in a standard electrochemical cell with a saturated calomel electrode (SCE) as a reference electrode and with a Pt mesh as an auxiliary electrode in sulfuric acid (Aldrich p.a.) with concentrations $c = 0.1$, 0.5, 1.0, 5.0, and 10 M, in Millipore water. The electrolytes were stirred mechanically. A computer-controlled linear sweep generator-potentiostat PG-30/1 (ASP-UŁ) was used for the initial electrochemical measurements [22].

The surface micrographs obtained using the SEM as well as a component analysis of the observed surface were carried out by means of EDX ISIS Link 300 Microanalysis with a Si(Li) detector (Oxford Instruments Microanalysis, UK). The Si(Li) detector worked at Mn K-line resolution, which guaranteed detection up to Be. The 1000 cps acquistition rate was 148 eV. The measurement system was coupled with a TESLA BS 340 scanning electron microscope.

The ECSTM/STM apparatus (Fig. 1) was designed and constructed in the Department of General and Inorganic Chemistry and in the Department of Solid State Physics of Łódź University. It is a combination of a STM apparatus for measurements under ambient conditions, modified for electrochemical applications. Surfaces within the range from 4.8 μm × 4.8 μm to 4.7 nm × 4.7 nm (1″ tube scanner, Staveley Sensors) and from 1.2 μm × 1.2 μm to 1.2 nm × 1.2 nm (0.5″ tube scanner) can be investigated. The apparatus was described in detail previously [10, 23].

The electrochemical part of the ESTM consists of an electrochemical unit in the STM block, a bipotentiostat-galvanostat module, and a scanner head with a special electrochemical cell ($V = 0.5$ cm^3). The bipotentiostat-galvanostat module is a modified apparatus, previously described [23]. This module is installed close to the scanner head, and assures the programmed values of electrode polarisation.

The electrochemical cell contained a reference electrode or a quasi-reference Pt electrode ($V_{q\text{-}ref}$) in the investigated electrolyte, a counter electrode as a Pt ring, and a working electrode (sample). The potential between the quasi-reference electrodes and the SCE reference electrode was measured independently, and the potential values in the investigated electrolytes were obtained as follows:

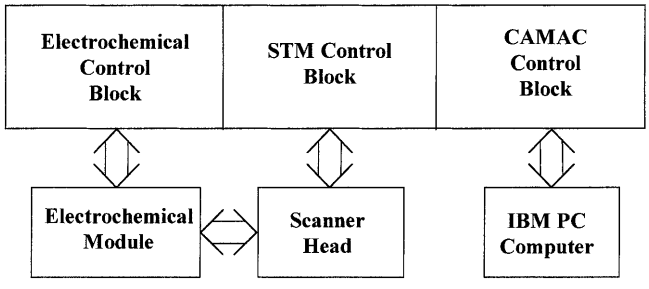

Fig. 1 A schematic representation of the ECSTM/STM measurement system. *CAMAC Control Block* – ensures – cooperation between the microcomputer and the CAMAC system; *STM Control Block* – 16 bit AD and DA converters and high voltage amplifiers for the control of *X*,*Y*,*Z* coordinates in the STM; *Electrochemical Control Block* – 16 bit DA converters for programming all electrochemical potentials and 16 bit AD converters for simultaneous measurements of the real potential and current of the working electrode; *Electrochemical Module* – analogous bipotentiostat-galvanostat device; *Scanner Head* – a typical STM scanner head with a special electrochemical four-electrode cell

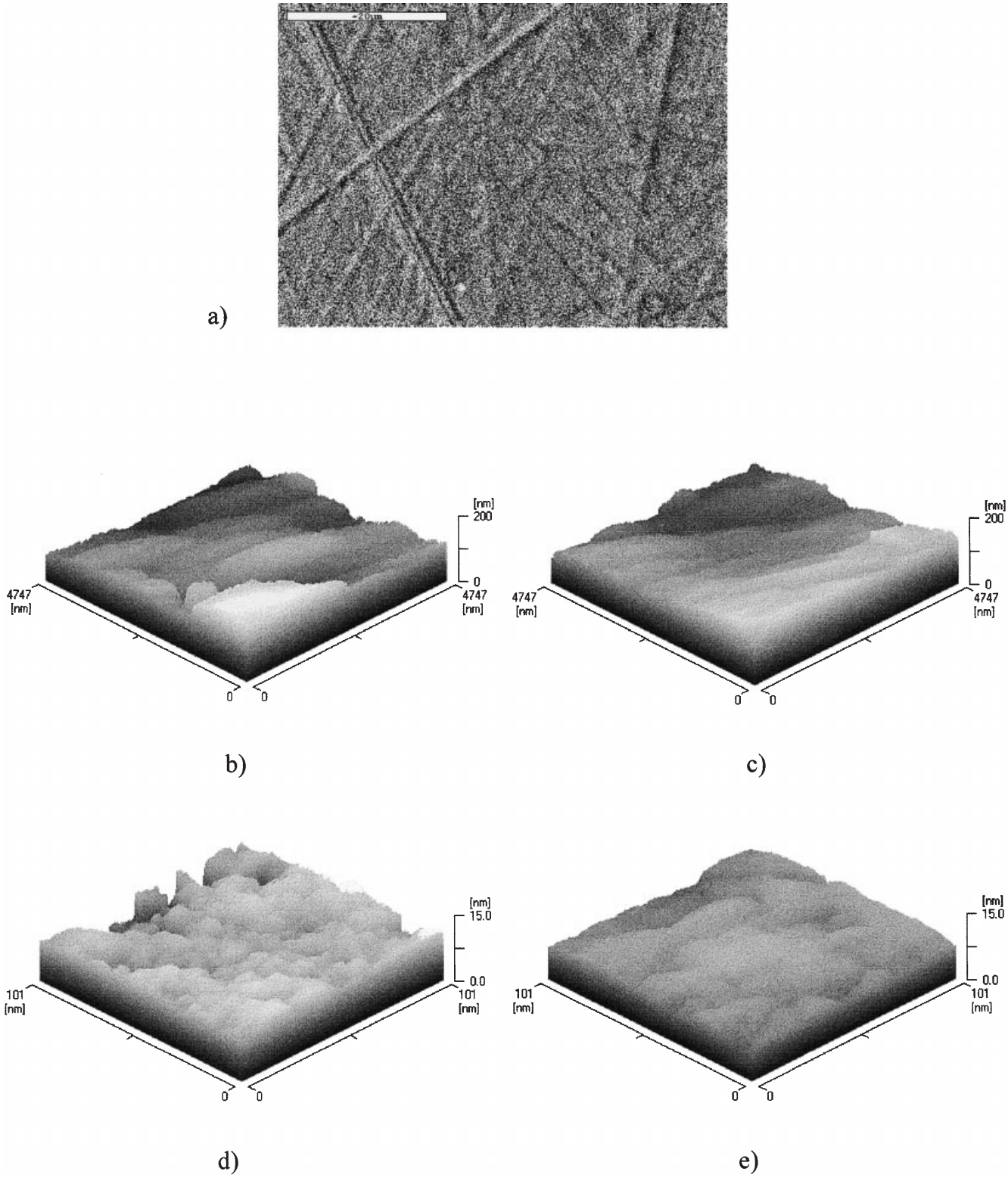

Fig. 2 The SEM micrographs and the STM topographies of the polycrystalline cobalt sample: **a** SEM micrograph after mechanical-chemical polishing, and the surface fragment of area 4800 nm × 4800 nm; **b** after mechanical polishing; **c** the same sample after mechanical and chemical polishing; **d** the same sample of area 100 nm × 100 nm after mechanical polishing; and **e** the same sample after mechanical and chemical polishing

[$E_{(q\text{-}ref)}$ (in 0.1 M H_2SO_4) − $E_{SCE} \cong 0.790$ V ± 0.030 V], [$E_{(q\text{-}ref)}$ (in 1.0 M H_2SO_4) − $E_{SCE} \cong 0.810$ V ± 0.030 V] and [$E_{(q\text{-}ref)}$ (in 10.0 M H_2SO_4) − $E_{SCE} \cong 0.840$ V ± 0.030 V]. The stability of the Pt quasi-reference electrode was controlled before and after each series of the experiments.

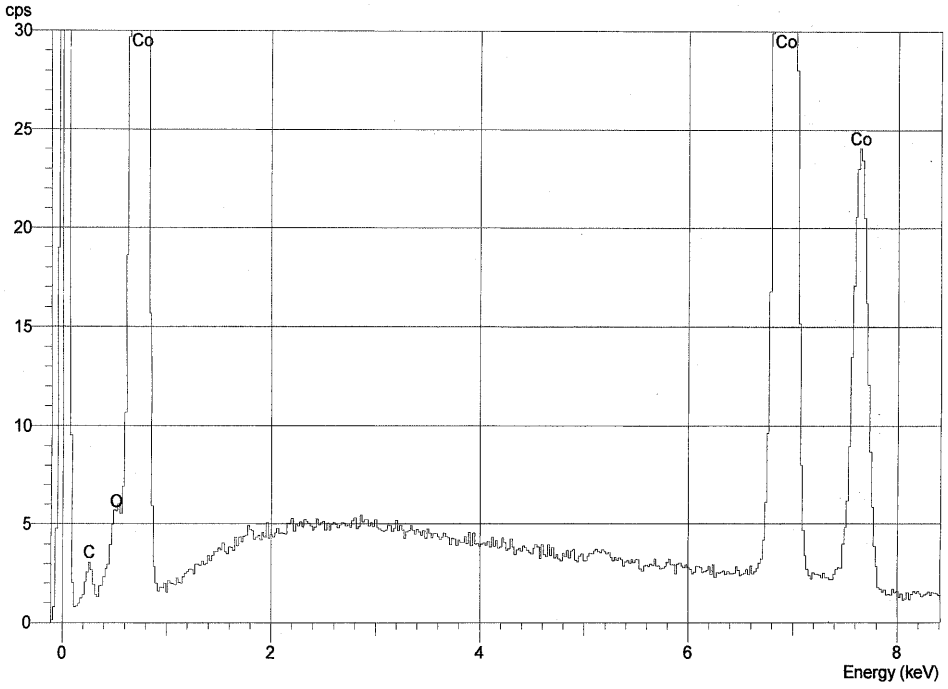

Fig. 3 The SEM-EDX quantitative analysis (standards: *C* $CaCO_3$; *O* quartz; *S* FeS_2; *Co* Co; 01/12/93, system resolution = 66 eV) of the cobalt|cobalt oxide electrode after mechanical-chemical polishing. Average composition of elements on the surface (at%): Co 87.4; O 1.87, Co:O ratio of ~47:1

The scanner tip was fastened to a stiff piezoceramics tube (Staveley Sensors). This construction provides very good stability and scan reproducibility, as well as low sensitivity to vibrations and mechanical shocks.

The ECSTM system was tested in 0.1 M H_2SO_4 using a HOPG basal place surface (ZYB, Union Carbide) as a standard with the carbon-carbon distance of 0.26 nm [24, 25].

The ECSTM/STM measurement procedure was based on the method described by Arvia and co-workers [18], with extensive modifications ensuring that the accuracy of the scans of the same fragment of the observed surface was ±10% at the 4800 nm × 4800 nm scale. The electrochemical experiment and the STM measurements are performed separately. In this procedure, ECSTM measurements were not exactly *in situ* but it was not exactly *ex situ*. We name it the ECSTM/STM method.

After polishing and cleaning of the sample, the first STM topography image was acquired ex situ on the dry sample surface. Then the STM tip was withdrawn, the cell was filled with the electrolyte solution and the sample connected as a working electrode. The single potential sweep was from −0.8 V to −0.15 or +0.1 V at the scan rate of 0.01 V s^{-1} applied to the working electrode. The potentiostat was switched to the open circuit regime, the electrolyte was pumped out, the cell rinsed with water, dried by argon and the second STM topography of the oxidised cobalt surface was acquired. Changes of the oxide layer were possible through rinsing with water. The same procedure was repeated for the sweep range −0.9 V to +0.2 V and with 20 s time delay at the final potential, to obtain STM images of the sample electrode at various potentials.

The STM images of the polycrystalline cobalt electrode after anodic polarisation in H_2SO_4 solutions (where the quasi-reference $Pt/V_{(q\text{-}ref)}$ electrodes were used in the investigated electrolytes) obtained in this work were as follows: (1) topography images of 4800 nm × 4800 nm were obtained first; they show the real picture of the electrode surface after mechanical-chemical or electrochemical treatment with a ±10% accuracy, and make it possible to observe the same surface fragment after different electrode treatments; (2) the 100 nm × 100 nm pictures illustrate the details in the centre of picture (1) which are discussed in this work; (3) the scales of the height of the profiles and of the 3D images were measured in relation to the bottom of the pictures. They do not present the absolute values of the oxide layer thickness. In order to interpret the anodic oxidation of the polycrystalline cobalt electrodes, the 100 nm × 100 nm images were used.

Results and discussion

The SEM supportive micrograph of the cobalt surface fragment after mechanical and chemical polishing is shown in Fig. 2a. The average SEM-EDX quantitative analysis of the elements at the surface gives a cobalt:oxygen ratio of ~47:1 (Fig. 3), and illustrates a relatively clean metallic polycrystalline cobalt surface.

It is characteristic of this experiment that using the SEM-EDX method of surface analysis the penetration of the electrons is to ~1 μm of depth, and the average results of the analysis illustrate the sum of the composition of ~1 μm of thickness of the cobalt sample|cobalt oxide layer covering it. For the thick cobalt oxide layer, the SEM-EDX surface analysis of the elements gives the most probable results. Carbon contamination of the surface is typical of the SEM-EDX analytical method, in which a vacuum diffusion pump is applied. This carbon contamination is treated as a background signal and can be neglected in the interpretation of the results.

The STM images, presented at different scales in Fig. 2b, d, illustrate the electrode surface after mechanical polishing only. Figure 2c, e shows the cobalt electrode surface after mechanical-chemical polishing. For the pictures presented at the 4800 nm × 4800 nm scale the influence of chemical polishing is illustrated in Fig. 2b, c. The chemical treatment of the rough and fine-

grained cobalt surface, shown in Fig. 2d, resulted in a relatively smooth electrode surface which is shown at the 100 nm × 100 nm scale in Fig. 2e. The electrode roughness is intermediately illustrated by the cross profiles and 3D images of the topography. Consequently, the procedure for the cobalt electrode pretreatment (mechanical polishing using the 2000 abrasive paper, rinsing in Millipore water, chemical polishing and drying in an argon stream) was applied in the experiment.

The initial $\log I = f(E)$ curves ($v = 0.01$ V s^{-1}) of the Co working electrodes in sulfuric acid aqueous solutions recorded in our experiments are shown in Fig. 4.

In dilute solutions of sulfuric acid (0.1 M) the activation current peaks and the well-defined passivation potential range are not visible. In 5.0 M sulfuric acid the activation current peak appears at $E_p \cong -0.10$ V_{SCE}, while the passivation region is registered from $E_{pass} > +0.10$ V_{SCE}. In the transpassivation region the current minimum is also observed at $E \cong +1.50$ V_{SCE}. The classical voltammetric activation-passivation curve has been obtained in a concentrated 10.0 M H_2SO_4 solution. A sharp activation current peak is observed at $E_p = -0.10$ V_{SCE}. The Tafel ratio ($dE/d \log I \cong 0.04$) characterises the region of the activation part of the anodic curve; a stable and large passivation potential region was observed from $E_{pass} = +0.30$ V_{SCE} up to $E = +1.75$ V_{SCE}, with high oxygen evolution overpotential on the cobalt oxide that is not discussed in this paper. However, it is interesting that the overpotentials of oxygen evolution on NiO_x and Co_3O_4 surfaces in acid solutions are similar [26]:

$$\eta_{NiO_x} \approx \eta_{Co_3O_4} \approx 0.30\,V_{SHE}$$

The enthalpies of transition are very different:

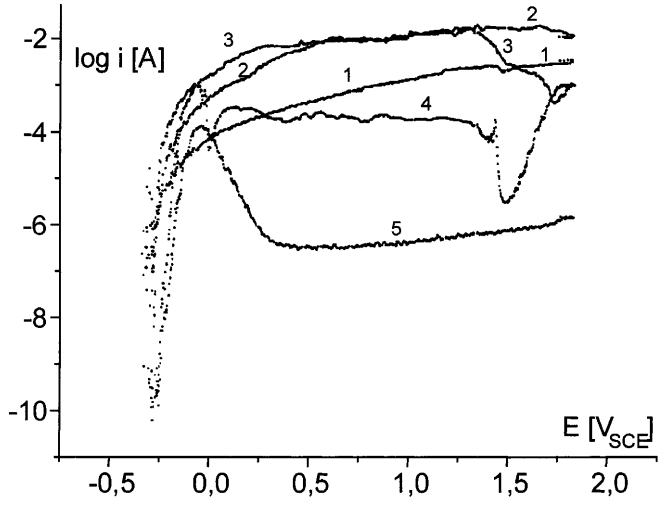

Fig. 4 The initial $\log I = f(E)$ curves ($v = 0.01$ V s^{-1}) of the Co electrode (after mechanical and chemical polishing) in H_2SO_4 stirred solutions at the concentrations (M): 0.1 (*1*); 0.5 (*2*); 1.0 (*3*); 5.0 (*4*); 10.0 (*5*)

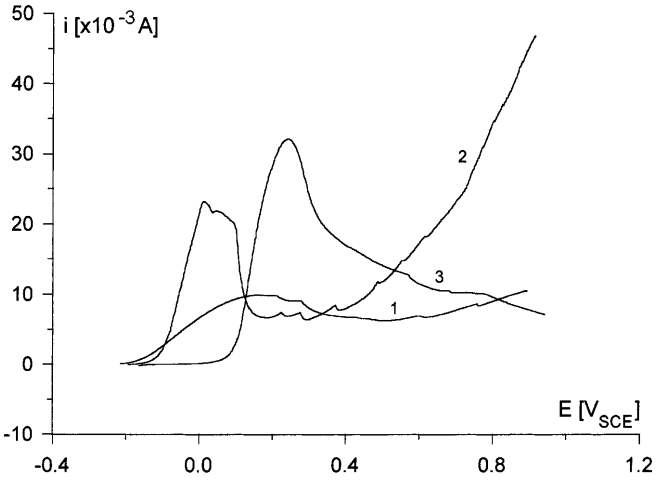

Fig. 5 The voltammetric curves ($v = 0.01$ V s^{-1}) of the polycrystalline cobalt electrodes obtained in ESTM cell in aqueous sulfuric acid solutions at the concentration (M): 0.1 (*1*); 1.0 (*2*); and 10.0 (*3*)

$$\Delta_t(H^\circ)_{NiO_x} \cong -0.5\ \text{kJ mol}^{-1};$$
$$\Delta_t(H^\circ)_{Co_3O_4} \cong -160\ \text{kJ mol}^{-1}$$

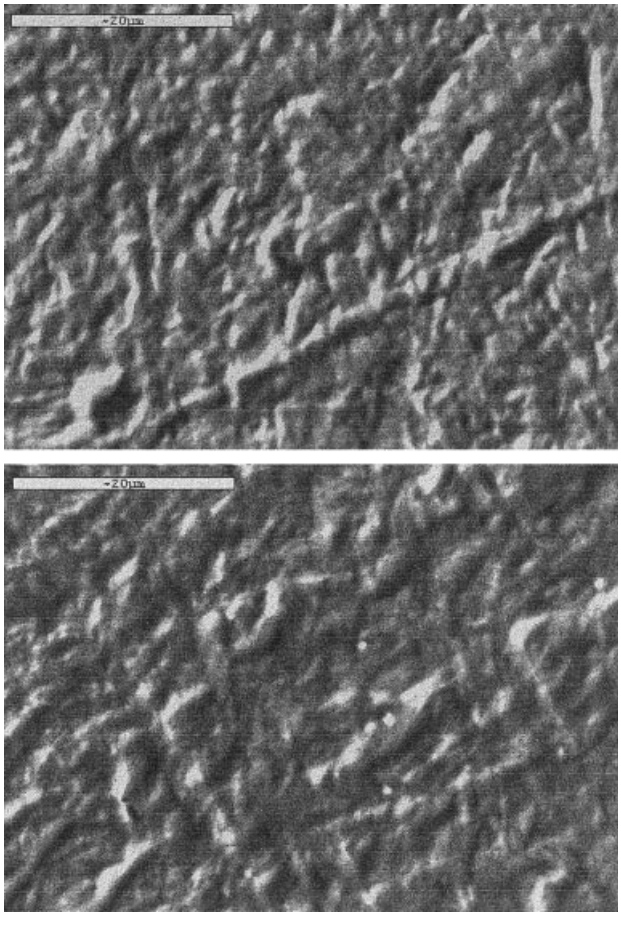

Fig. 6 a,b

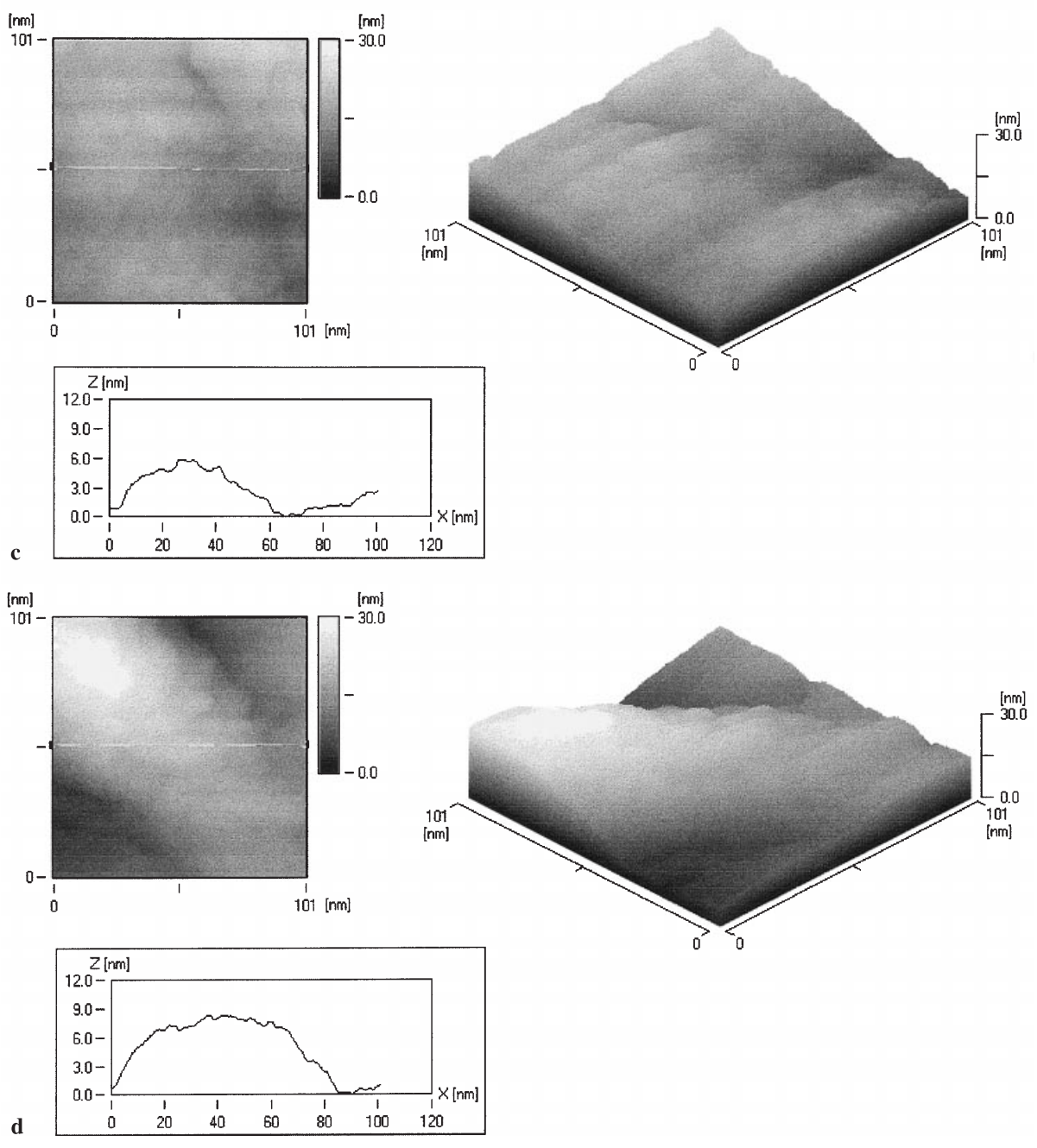

Fig. 6 The electrooxidation of the polycrystalline cobalt electrode in 0.1 M H_2SO_4: **a** the SEM micrographs after the first anodic scan ($v = 0.01$ V s^{-1}) from -0.01 V_{SCE} up to $+0.89$ V_{SCE}; **b** after oxidation at $+0.89$ V_{SCE} ($\tau = 20$ s), $Q = +1050$ mC, and the STM images: **c** the STM topography after the first anodic scan, **d** after $\tau = 20$ s of anodic oxidation at $E = +0.89$ V_{SCE}; Pt(90)Ir(10) tip, $E_T = +0.4$ V, $I_T = +1.0$ nA

The oxygen evolution in acids takes place on Co_3O_4, when E is in the range of 1.69–1.79 V_{SCE}, together with corrosion and dissolution of the oxide layer. The results obtained in this experiment are in accordance with the literature data [17].

In the anodic potential range from $E \cong -0.25$ V_{SCE} up to $E \cong -0.04$ V_{SCE}, which is characteristic of the active dissolution of cobalt (Fig. 4), the non-autocatalysed reaction mechanism is analogous to that of iron [27], and can be described as follows (Eqs. 1–8):

$$Co + H_2O \rightleftharpoons Co(H_2O)_{ad} \quad (1)$$

$$Co(H_2O)_{ad} \rightleftharpoons Co(OH^-)_{ad} + H^+ \quad (2)$$

$$Co(OH^-)_{ad} \rightleftharpoons (CoOH)_{ad} + e^- \quad (3)$$

$$Co + H_2O \rightleftharpoons (CoOH)_{ad} + H^+ + e^- \quad (4)$$

$$(CoOH)_{ad} \overset{RDS}{\rightleftharpoons} CoOH^+ + e^- \quad (5)$$

$$CoOH^+ + H^+ \rightleftharpoons Co^{2+} + H_2O \quad (6)$$

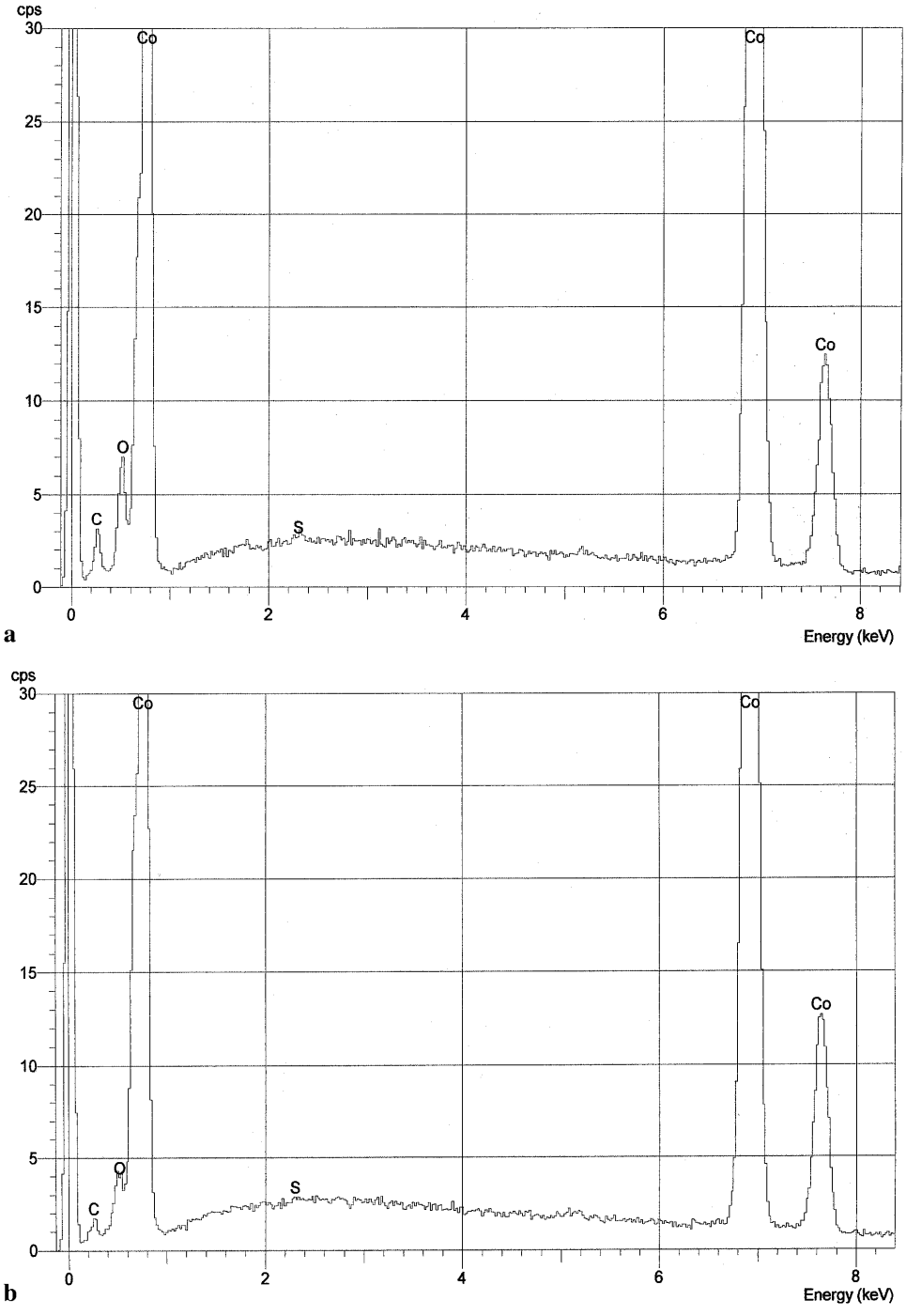

Fig. 7 The results of the SEM-EDX quantitative analysis of the Co surface after various electrochemical treatments in 0.1 M H_2SO_4: **a** after the first anodic cycle ($v = 0.01$ V s^{-1}) from −0.01 V_{SCE} up to +0.89 V_{SCE}, with an average composition of elements on the surface of (at%): S 0.12, Co 83.7, O 5.70; **b** after anodic oxidation at $E = +0.89$ V_{SCE} ($\tau = 20$ s), with an average composition of elements on the surface of (at%): S 0.65, Co 32.00, O 32.00

and

$$CoOH^{+}.....SO_4^{2-} \rightleftharpoons (CoOH \cdot H^{+} \cdot \ SO_4^{2-}) \quad (7)$$

$$Co(OH^{-})_{ad} + CoOH^{+} \longrightarrow 2CoO + 2H_{ad} \quad (8)$$

However, Trasatti and Lodi's suggestion [17] that in acid solutions the primary water molecule increases the rate determining step must be also remembered. Hence, in reality, the surface layer of the initially passivated cobalt is the CoO surface layer with SO_4^{2-} anions, with protons, and with the inclusion of hydrogen atoms.

For a Co_3O_4 spinel formed electrochemically the potential limits and the frequency of a perturbing potential as well as the electrolyte composition play a decisive role [28, 29].

The development of model theories of the oxide electrical double layer plays an important role in modern

electrochemical research. Petrii [12] proposed the metal|metal oxide|electrolyte solution boundary phase and a corresponding simplified model. In this model the adsorption capacitance and the capacitance modelling of the oxide volume properties, as well as oxide metal interface capacitance, play important roles.

The voltammetric curves of a cobalt electrode that were obtained in an ECSTM cell with H_2SO_4 solutions of different concentrations (c = 0.1, 1.0 and 10.0 M) are shown in Fig. 5. The voltammetric curve of the cobalt electrode in 0.1 M H_2SO_4 (Fig. 5a, curve 1) is characterised by a flattened current activation peak at $E_p \cong +0.15$ V_{SCE}; the passivation potential (E_{pass}) was placed in the range from $+0.30$ V_{SCE} up to $+0.80$ V_{SCE}.

The cobalt surface obtained in 0.1 M sulfuric acid solution was measured by means of the SEM-EDX apparatus. The SEM micrographs of this surface are shown in Fig. 6a, b. Fragments of these surfaces are presented as the STM images at a scale of 100 nm × 100 nm (Fig. 6c, d). After the first voltammetric scan in 0.1 M H_2SO_4 the cobalt electrode was oxidised (Fig. 6a) and it can be compared with the clean cobalt surface illustrated in Fig. 2a. Figure 6b illustrates the SEM micrograph of the oxidised cobalt electrode in 0.1 M H_2SO_4 after the anodic cycle from -0.8 $V_{q\text{-}ref}$ up to $+0.1$ $V_{q\text{-}ref}$ and τ = 20 s of coulometric oxidation. The cobalt:oxygen average ratio (~14.7:1) demonstrated a thin layer of cobalt oxide with irregular islands of the cobalt oxide developed on the cobalt surface (Fig. 7a).

The coulometric oxidation of the cobalt electrode at $+0.1$ $V_{q\text{-}ref}$ (τ = 20 s) in 0.1 M. H_2SO_4 built an irregular and thick cobalt oxide layer (Fig. 6b), with the Co:O ratio of ~1:1 (Fig. 7b) being the result of the qualitative surface analysis of the elements.

The STM pictures presented in Fig. 6c, d show a fragment of the surface at 100 nm × 100 nm the scale. These pictures show clearly the increase of the cobalt oxide layer.

It is obvious that on the polycrystalline cobalt surface we did not observe any regular lattice forms at the nanometric scale, similar to those observed on the monocrystals presented at an atomic scale by Itaya and co-workers [20].

In 1.0 M H_2SO_4 the current activation peak is doubled (Fig. 5) at $E_p = +0.01$ V_{SCE}. This doubled current peak suggests hydrogen desorption or the two-step anodic dissolution reaction Co ⇒ Co(II) ⇒ Co(III). A relatively narrow passivation potential region is observed within the limited range from $E = +0.14$ V_{SCE} up to $E = +0.45$ V_{SCE}. In this region, current oscillations, characteristic of a cobalt electrode in a sulfuric acid solution, were also observed [22].

The anodic oxidation of the cobalt electrode at $E = +0.1$ $V_{q\text{-}ref}$ and within τ = 20 s brought the Co:O ratio to ~16:1. That atomic ratio is comprehensible because of the transpassivation processes taking place at this electrode potential.

The anodic oxidation of the Co electrode was carried out at $E = -0.15$ $V_{q\text{-}ref}$. The SEM micrograph of the cobalt surface after the first voltammetric cycle from 0.8 to -0.15 $V_{q\text{-}ref}$ is shown in Fig. 8a, and the same electrode surface, after the coulometric oxidation at $E = -0.15$ $V_{q\text{-}ref}$, is presented in Fig. 8b. The fragments of the variously oxidised Co electrode are shown in Fig. 8c, d as STM images at the 100 nm × 100 nm scale. The short range of the passivation potential and the passivation current oscillations (Fig. 5) show poor reproducibility of the results of the SEM-EDX surface analysis of the elements. It is important that the anodic charge in 1.0 M H_2SO_4 is the largest in relation to more diluted and to more concentrated sulfuric acid solutions. The "agent" responsible for the consumption of about 700 mC has not been identified. It is possible that parasitic, uncontrolled cobalt electrodissolution takes place. Hence, the 1.0 M H_2SO_4 solution cannot be recommended as a medium for obtaining a stable and reproducible CoO layer as a final result.

In the concentrated 10.0 M H_2SO_4 solution the voltammetric curve is characterised by a single and sharp activation current peak at $E_p = +0.24$ V_{SCE}, and a large passivation potential region from $E_{pass} = +0.35$ V_{SCE} (Fig. 5). Anodic oxidation of the cobalt samples at $E = +0.94$ V_{SCE} was used for STM and SEM-EDX observations. The SEM micrographs of a

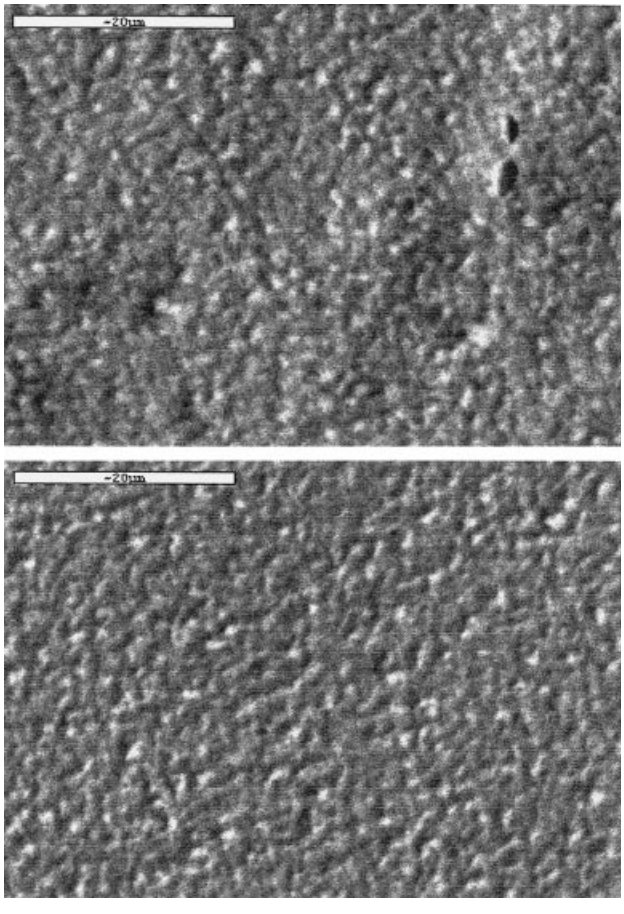

Fig. 8 a, b

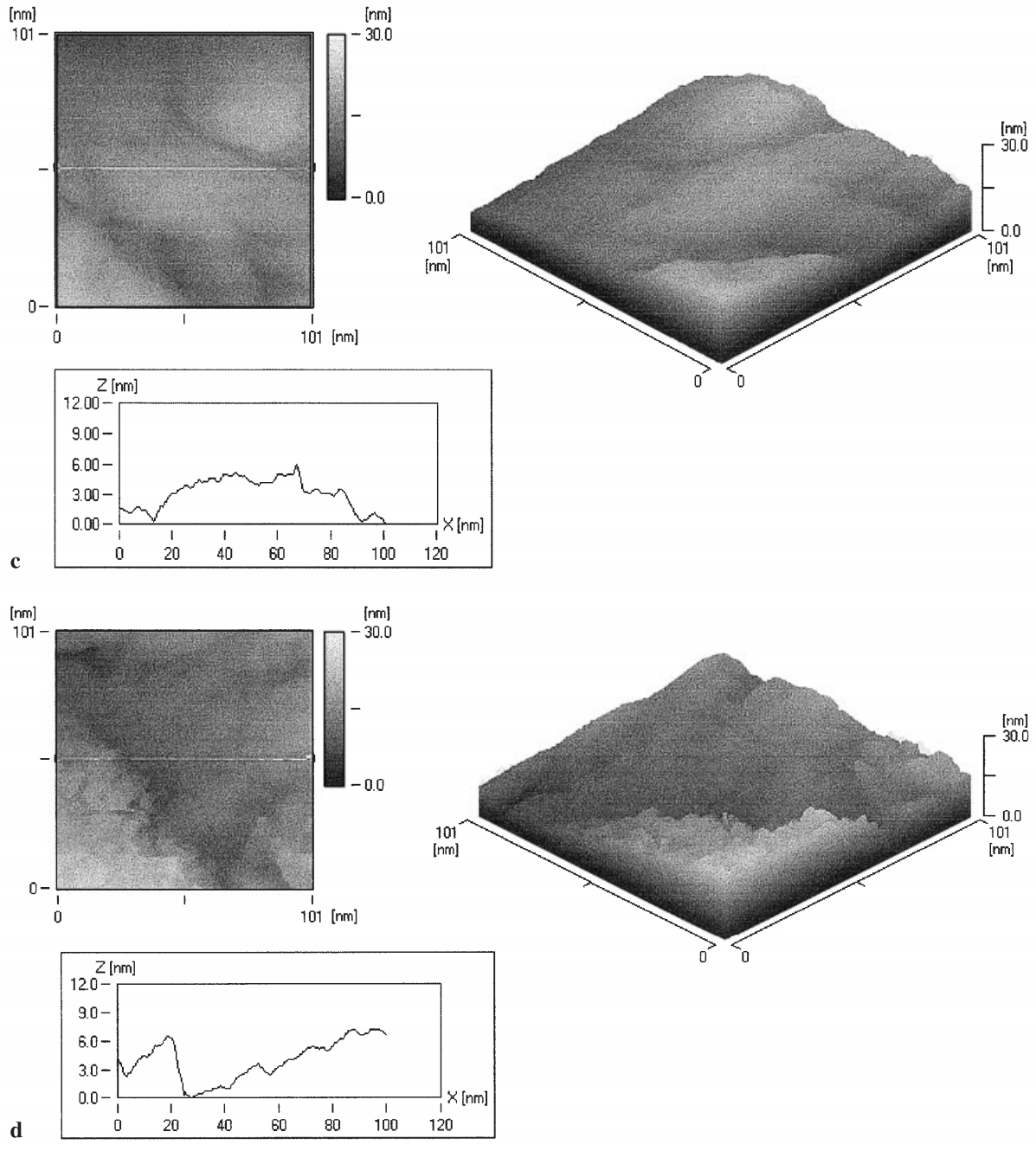

Fig. 8 The electrooxidation of the polycrystalline Co electrode in 1.0 M H_2SO_4: **a** the SEM micrographs after the first anodic scan ($v = 0.01$ V s^{-1}) from $+0.01$ V_{SCE} up to $+0.66$ V_{SCE}; **b** after the first scan and $\tau = 20$ s electrooxidation at $+0.66$ V_{SCE}; and the STM images of the same electrode: **c** after the first anodic scan, and **d** the coulometric oxidation ($Q = +1860$ mC); Pt(90)Ir(10) tip, $E_T = 0.4$ V, $I_T = +1.0$ nA

cobalt surface and of an oxidised cobalt surface are shown in Fig. 9.

After the first voltammetric scan in 10.0 M H_2SO_4 the cobalt oxide layer covered the cobalt electrode surface epitaxially (Fig. 9a and c) and a cobalt:oxygen ratio of 1:1 was obtained as early as the first voltammetric cycle. The irregularity of this oxide layer takes the shape of holes presented as the white points in Fig. 9a. After coulometric oxidation at a controlled potential ($E = +0.1$ $V_{q\text{-}ref}$, $\tau = 20$ s) the thickness of the CoO layer increases and the oxide layer consists of well-developed densely packed grains (Fig. 9b).

The pictures in Fig. 9c, d illustrate the central fragments of the surfaces presented in Fig. 9a, b, respectively. The profile presented in Fig. 9c shows semi-regular wool-form topography (Fig. 9c) with the height of "wools" about 6 nm at the relative scale. After anodic oxidation at $E_{pass} = +0.1$ $V_{q\text{-}ref}$ ($Q = 1250$ mC) the individual "wool" forms take the shape of large and flat spherical planes with a relative height of about 3 nm

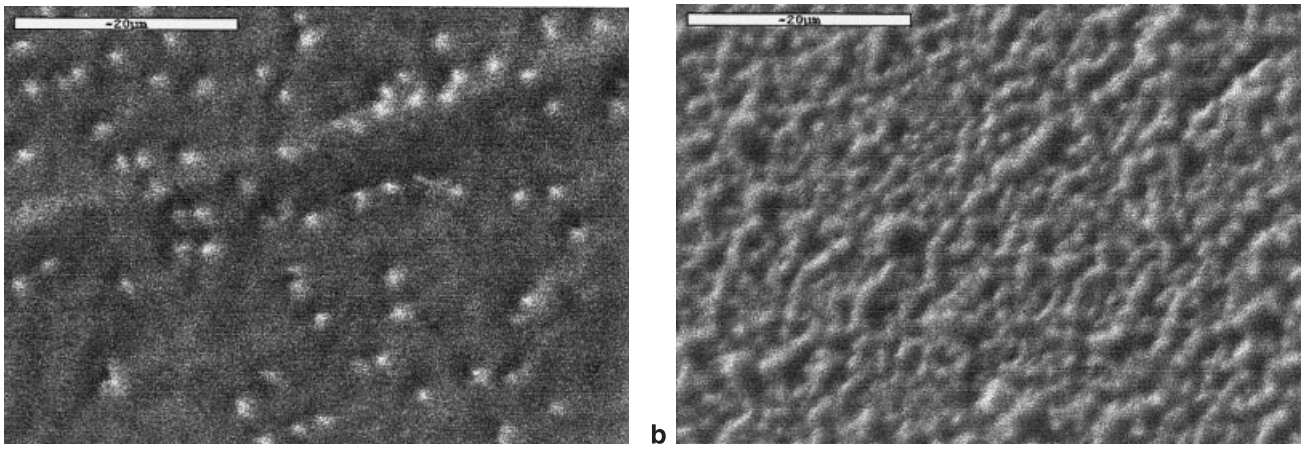
a
b

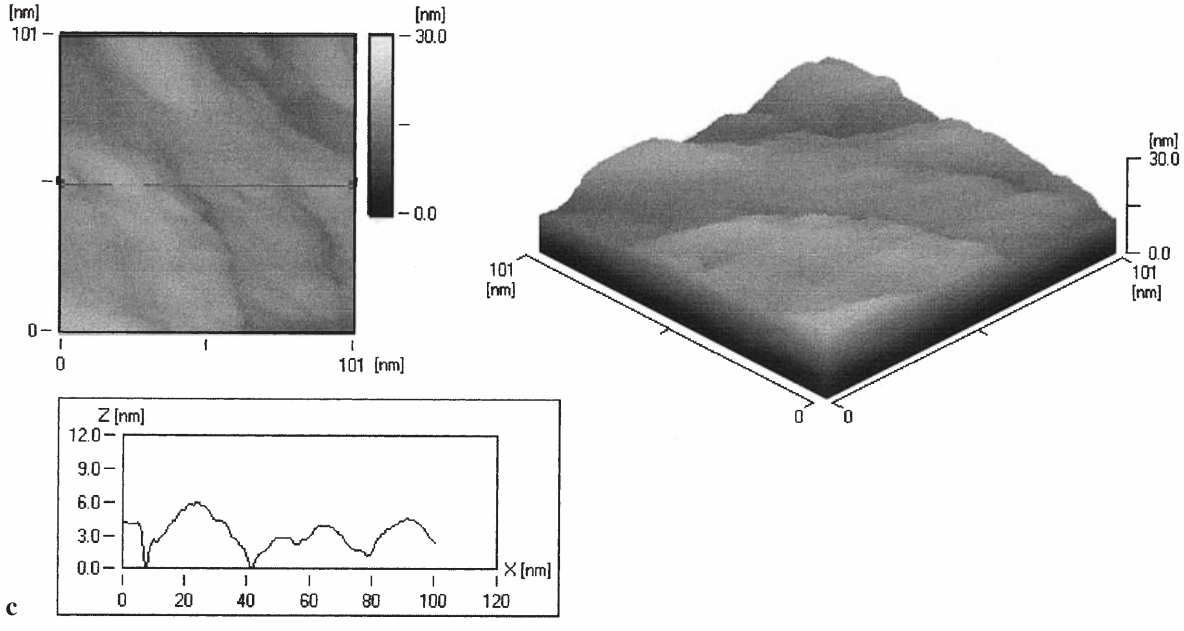
[nm]
101
[nm]
30.0
0.0
0
101 [nm]
[nm]
30.0
0.0
101
[nm]
101
[nm]
0
0
Z [nm]
12.0
9.0
6.0
3.0
0.0
X [nm]
0
20
40
60
80
100
120
c

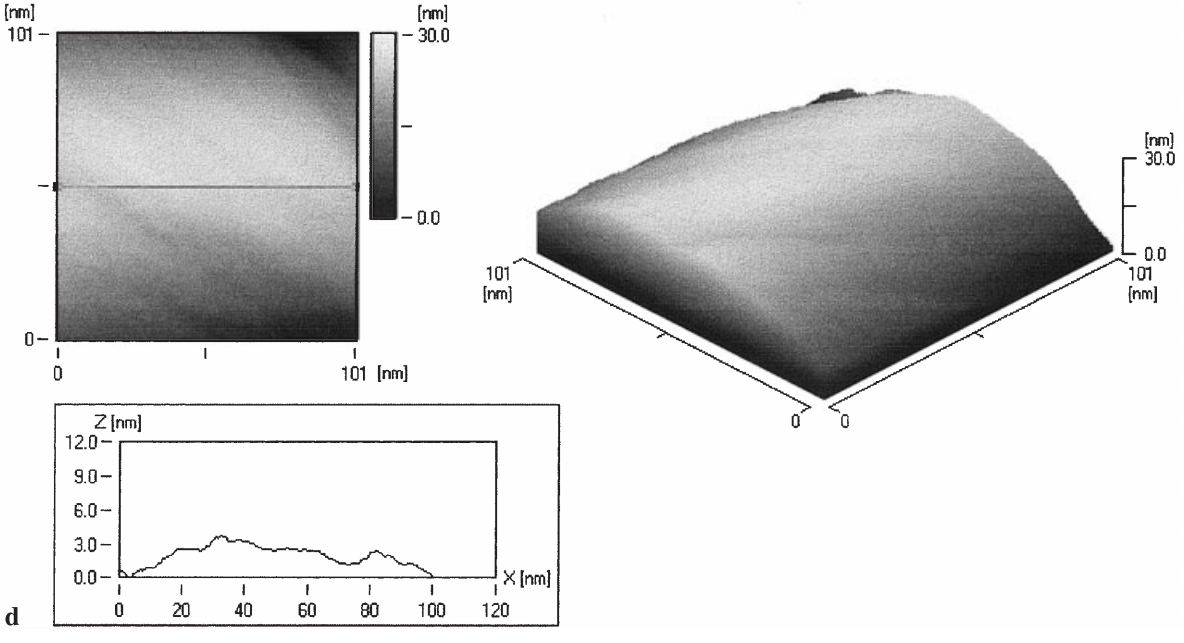
[nm]
101
[nm]
30.0
0.0
0
101 [nm]
[nm]
30.0
0.0
101
[nm]
101
[nm]
0
0
Z [nm]
12.0
9.0
6.0
3.0
0.0
X [nm]
0
20
40
60
80
100
120
d

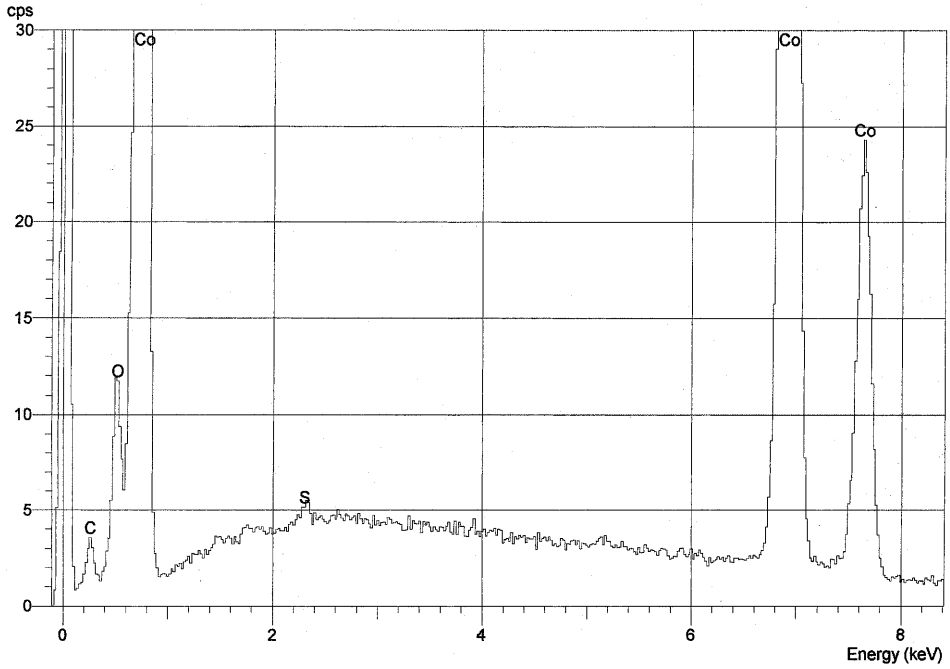

(Fig. 9d). The SEM-EDX final results of the surface analysis, which are presented in the legend to Fig. 10, give the reasons for using the 10.0 M H_2SO_4 electrolyte for Co oxidation and for obtaining a relatively smooth and stable cobalt oxide layer covering the polycrystalline cobalt electrode.

Additionally, the results of the quantitative microanalysis of the surfaces showed that the average concentrations of sulfur in the surface layer increase with anodic oxidation of the cobalt electrode, proportionally to the electric charge. This result is in agreement with the cobalt electrooxidation mechanism mentioned above, in Eqs. 7 and 8.

Fig. 10 The SEM-EDX spectra of the cobalt|cobalt oxide electrode obtained in 10.0 M H_2SO_4 solution after anodic electrooxidation at $E_{pass} = +0.94\ V_{SCE}$ and $\tau = 20$ s, ($Q = 1250$ mC); average concentration of the elements (at%): S 0.71, Co 26.97, O 26.97; Co:O ratio of 1:1

Conclusions

1. Under coulometric control, the anodic oxidation at the passivation potentials of polycrystalline cobalt electrodes in aqueous solutions of sulfuric acid of concentrations of 0.1 M and 10.0 M cause the formation of cobalt oxide layers of wool-like forms with a cobalt:oxygen ratio of 1:1.
2. The changes of the topography of the polycrystalline cobalt electrode surface show significant differences after the first anodic polarisation cycle, which were observed in the SEM micrographs and the STM images in different scales. The new observed oxide structures have little relation to the bare metal topography. The topography of electrochemically formed cobalt oxide depends on active centres at the polycrystalline cobalt electrodes.
3. The anodic oxidation of polycrystalline cobalt electrodes in dilute or concentrated sulfuric acid solutions at a stable passivation potential produces a simple cobalt oxide with the CoO formula, without the Co_3O_4 spinel product.

Acknowledgements This work was supported by Grant No. 7 T 08C 042 11, awarded by the Polish State Committee of Scientific Research, and by Łódź University Individual Grant No 505/650.

◀

Fig. 9 The electrooxidation of a polycrystalline Co electrode in 10.0 M H_2SO_4: **a** the SEM micrographs after the first anodic scan ($v = 0.01\ V\ s^{-1}$) from $+0.04\ V_{SCE}$ up to $+0.94\ V_{SCE}$; **b** after electrooxidation ($\tau = 20$ s , $E_{pass} = +0.94\ V_{SCE}$); and the STM images at a scale of 100 nm × 100 nm after **c** the first anodic scan (from $+0.04\ V_{SCE}$ up to $+0.94\ V_{SCE}$) and **d** after $\tau = 20$ s electrooxidation at $E_{pass} = +0.94\ V_{SCE}$ ($Q = 1250$ mC); Pt(90)Ir(10) tip, $E_T = +0.4$ V, $I_T = +1.0$ nA

References

1. Bard AJ, Fu-ren Fon F (1993) Application in electrochemistry. In: Bonnell DA (ed) Scanning tunneling microscopy and spectroscopy. Theory, techniques and applications. VCH, New York, pp 287–333
2. Siegenthaler H (1992) STM in electrochemistry. In: Wiesendanger R, Güntherodt H-J (eds) Scanning tunneling microscopy, vol 2. Springer, Berlin Heidelberg New York pp 7–49
3. Itaya K (1993) In situ scanning tunneling microscopy of electrode/solution interface. In: Masuko N, Osaka T, Fukunaka Y (eds) New trends and approaches in electrochemical technology. VCH, Tokyo, pp 181–193
4. Yu ET (1997) Chem. Rev 97: 1017–1044
5. Hwang RQ, Bartlet MC (1997) Chem Rev 97: 1063–1082
6. Chiang S (1997) Chem Rev 97: 1083–1094
7. Poirier GE (1997) Chem Rev 97: 1117–1127

8. Gewirth AA, Niece BK (1997) Chem Rev 97: 1129–1162
9. Nyffenegger RM, Penner RM (1997) Chem Rev 97: 1195–1230
10. Błaszczyk T, Krzyczmonik P, Kaźmierczak D, Scholl H (1998) Pol J Chem 72: 2134
11. Shohat I, Mandler D (1994) J Electrochem Soc 141: 995
12. Petrii OA (1996) Electrochim Acta 41: 2307
13. Trasatti S (1971) Chim Ind (Milan) 53: 559
14. Tarasevic MR, Efremov BR (1980) Properties of spinel-type oxide electrodes. In: Trasatti S (ed) Electrodes of conductive metallic oxides, part A. Elesevier, Amsterdam, pp 221–239
15. Sokolovski VD (1990) Catal Rev Sci Eng 32: 1
16. Arvia AJ, Canullo JC, Custidiano E, Perdriel CL, Triaca WE (1986) Electrochim Acta 31: 1359
17. Trasatti S, Lodi G (1981) Oxygen and chlorine evolution at conductive metallic oxide anodes. In: Trasatti S (ed) Electrodes of conductive oxides, part B. Elsevier, Amsterdam, pp 521–570
18. Kessler T, Visintin A, Triaca WE, Arvia AJ, Genero di Clavo MR (1991) J Appl Electrochem 21: 516
19. Maruyama T, Arai S (1996) J Electrochem Soc 143: 1383
20. Ando S, Suzuki T, Itaya K (1997) J Electroanal Chem 431: 277
21. Dettner HW, Elze J (1966) Handbuch der galvanotechnik. Hanser, Munich
22. Scholl H, Hofman B, Kupis J, Polañski K (1994) Electrochim Acta 39: 115
23. Błaszczyk T, Olejniczak W, Kobierski P (1995) Pomiary Automatyka Kontrola 12: 342
24. Lev O, Fan F-R, Bard AJ (1988) J Electrochem Soc 135: 783
25. Ando S, Suzuki T, Itaya K (1996) J Electroanal Chem 412: 139
26. Trasatti S (1994) Transition metal oxides: versatile materials for electrocatalysis. In: Lipkowski J, Ross PN (eds) The electrochemistry of novel materials. VCH, Wienheim, pp 207–293
27. Belluci F, Farina CA, Faita G (1981) Electrochim Acta 26: 731
28. Ord JL, De Smet DJ, Beckstead DJ (1989) J Electrochem Soc, 136: 2178
29. Baggio R, Carugati A, Trasatti S (1987) J Appl Electrochem, 17: 828